

Biosynthetic isotope fractionation negligibly impacts biomarker ^{14}C ages

Jordon Hemingway¹

¹Harvard University

November 22, 2022

Abstract

Radiocarbon (^{14}C) ages of acetogenic lipid biomarkers such as n-alkanes are a powerful tool to track carbon-cycle turnover times. In sediments, biomarker ages are almost always older than the depositional age due to reservoir effects. Recently, Lane et al. [2021, Anomalously low radiocarbon content of modern n-alkanes, *Organic Geochemistry* 152, 104170] reported ^{14}C ages up to [?]1500 yr for n-alkanes extracted from leaf tissue of living plants; they attributed this apparent “pre-aging” to biosynthetic fractionation against ^{14}C . However, reported ^{14}C ages are always corrected for mass-dependent fractionation using a $^{14}\text{C}/^{13}\text{C}$ mass law, b , of 2.0. Lane et al.’s interpretation therefore requires that lipid biosynthesis follows large, anomalous deviations from mass-dependent fractionation, with b reaching values as high as [?] 124. Here, I test this assumption by estimating kinetic and equilibrium mass laws for various processes involved in acetogenic lipid biosynthesis using simple approximations and more robust computational chemistry methods. I find that kinetic b values range from 1.880 to 1.995 and that equilibrium b values for several chain elongation steps range from 1.856 to 1.880, consistent with previous results for other chemical and biological processes. In contrast, complex reaction networks may lead to large expressed b values, but only when $\ln(13\alpha) - 0$. Combined, these results imply maximum ^{14}C age offsets due to biosynthetic fractionation of 20 to 40 yr. Biomarker ^{14}C ages are therefore robust to biosynthetic isotope fractionation and can be confidently interpreted to reflect carbon-cycle turnover times.

1 Highlights

2 **Biosynthetic isotope fractionation negligibly impacts biomarker ^{14}C ages**

3 Jordon D. Hemingway

- 4 • Acetogenic lipid biosynthesis follows mass-dependent carbon isotope fractionation
- 5 • Acetogenic lipid biosynthesis $^{14}\text{C}/^{13}\text{C}$ mass laws range from $b \approx 1.87$ to $b \approx 1.97$
- 6 • Non-canonical mass-laws are only expressed when ^{13}C fractionation is negligibly small
- 7 • Fractionation cannot explain anomalously old *n*-alkane ^{14}C ages

Biosynthetic isotope fractionation negligibly impacts biomarker ^{14}C ages

Jordon D. Hemingway^{a,b,1,*}

^aDepartment of Earth and Planetary Sciences, Harvard University, Cambridge, MA, USA

^bGeological Institute, Department of Earth Sciences, ETH Zürich, Zürich, Switzerland

Abstract

Radiocarbon (^{14}C) ages of acetogenic lipid biomarkers such as *n*-alkanes are a powerful tool to track carbon-cycle turnover times. In sediments, biomarker ages are almost always older than the depositional age due to reservoir effects. Recently, Lane et al. [2021, Anomalously low radiocarbon content of modern *n*-alkanes, *Organic Geochemistry* **152**, 104170] reported ^{14}C ages up to ≈ 1500 yr for *n*-alkanes extracted from leaf tissue of living plants; they attributed this apparent “pre-aging” to biosynthetic fractionation against ^{14}C . However, reported ^{14}C ages are always corrected for mass-dependent fractionation using a $^{14}\text{C}/^{13}\text{C}$ mass law, *b*, of 2.0. Lane et al.’s interpretation therefore requires that lipid biosynthesis follows large, anomalous deviations from mass-dependent fractionation, with *b* reaching values as high as ≈ 124 . Here, I test this assumption by estimating kinetic and equilibrium mass laws for various processes involved in acetogenic lipid biosynthesis using simple approximations and more robust computational chemistry methods. I find that kinetic *b* values range from 1.880 to 1.995 and that equilibrium *b* values for several chain elongation steps range from 1.856 to 1.880, consistent with previous results for other chemical and biological processes. In contrast, complex reaction networks may lead to large expressed *b* values, but only when $\ln(^{13}\alpha) \rightarrow 0$. Combined, these results imply maximum ^{14}C age offsets due to biosynthetic fractionation of ~ 20 to 40 yr. Biomarker ^{14}C ages are therefore robust to biosynthetic isotope fractionation and can be confidently interpreted to reflect carbon-cycle turnover times.

Keywords: radiocarbon, mass-dependent fractionation, biomarkers

1. Introduction

Natural-abundance radiocarbon (^{14}C) activity represents a powerful geochronometer, with applications ranging from tracking of various carbon-cycle turnover times and reservoir ages to precise and accurate dating of sediments and anthropological artifacts. The utility of radiocarbon comes from its ubiquity; ^{14}C is incorporated into all inorganic and organic carbon (OC) phases. Of particular interest here is ^{14}C age measurement of specific lipid compounds—termed “biomarkers”—extracted from complex OC mixtures. Because a given biomarker is produced by a particular

*Corresponding author

Email address: jhemingway@ethz.ch (Jordon D. Hemingway)

20 group of organisms or biosynthetic/chemical pathway, its ^{14}C age offers insight into specific carbon-cycle processes
21 that cannot be elucidated by the bulk OC age, which integrates signals from multiple sources. Since the advent of this
22 technique by Eglinton et al. (1996), ^{14}C ages of multiple biomarker classes—for example, acetogenic plant-waxes
23 (*n*-alkanes, *n*-alcohols, and *n*-alkanoic acids), isoprenoid archaeal lipids, lignin phenols, and condensed aromatic
24 hydrocarbons—have been utilized to elucidate a broad suite of carbon-cycle processes, including: soil carbon turnover
25 times, both in modern settings and in response to past climatic perturbations (Eglinton et al., 2021; Hein et al., 2020;
26 Hemingway et al., 2018; Smittenberg et al., 2006); permafrost thaw (Feng et al., 2013); condensed aromatic (“black”)
27 carbon cycling (Coppola et al., 2018); marine sediment chronologies (Eglinton et al., 1997; Pearson and Eglinton,
28 2000); and microbial metabolisms (Ingalls et al., 2006; Petsch et al., 2001); among others.

29 Like all geochronometers, the utility of biomarker radiocarbon requires that ^{14}C ages are unaffected by kinetic
30 and equilibrium processes that fractionate carbon isotopes and thus exclusively reflect the time that has passed since
31 each compound was biosynthesized (after accounting for temporal changes in atmospheric ^{14}C inventory). This
32 is accomplished by the practice of correcting measured ^{14}C activity for isotope fractionation using concomitantly
33 measured $^{13}\text{C}/^{12}\text{C}$ ratios and assuming that fractionation is mass dependent (e.g., Stuiver and Polach, 1977). Following
34 Craig (1954), fractionation corrections typically use a $^{14}\text{C}/^{13}\text{C}$ mass law, here termed *b*, of 2.0; that is, reported
35 ages inherently assume that ^{14}C fractionates exactly twice as much as ^{13}C for any given process since the $^{14}\text{C}/^{12}\text{C}$
36 mass difference is roughly double that of the $^{13}\text{C}/^{12}\text{C}$ mass difference. Early work estimated the $^{14}\text{C}/^{13}\text{C}$ mass laws
37 for various kinetic and equilibrium chemical reactions both theoretically and experimentally (e.g., Bigeleisen, 1952;
38 Bigeleisen and Wolfsberg, 1953; Bigeleisen, 1949; Stern and Vogel, 1971); nearly all processes measured to date are
39 described by a mass law of $b \in (1.8, 2.0)$, here termed the “canonical range”. Although most processes cluster around
40 $b = 1.9$ rather than the *reference line* value of $b_{\text{RL}} = 2.0$ used when reporting radiocarbon ages, resulting age biases
41 caused by this difference have been shown to be less than or near ^{14}C analytical uncertainty (Wigley and Muller, 1981;
42 Stuiver and Robinson, 1974; Southon, 2011; Fahrni et al., 2017; Steier et al., 2004). Thus, deviations from b_{RL} are
43 often ignored and reported ^{14}C ages are considered unbiased.

44 Despite this established practice, Lane et al. (2021) recently extracted long-chain *n*-alkanes from the leaves of
45 living plants and found biomarker ^{14}C ages that are up to ≈ 1500 yr older than bulk leaf tissue. They argued against
46 contamination by ^{14}C -free (“dead”) carbon—for example from solvent extraction or chemical processing steps—and
47 instead interpret this “pre-aging” as a result of large, anomalous fractionation against ^{14}C during lipid biosynthesis.
48 Because of this, they conclude that biomarkers violate a fundamental assumption of the radiocarbon geochronometer
49 and urge caution when interpreting their ^{14}C ages. If true, this result would represent a major setback to the burgeoning
50 compound-specific radiocarbon field and would possibly invalidate several recent carbon-cycle insights that have been
51 elucidated using biomarker ^{14}C age measurements. This interpretation therefore warrants critical examination.

52 Here, I evaluate the Lane et al. (2021) hypothesis by focusing specifically on the plausibility of calculated *b* values
53 that would be required to explain these data. Because multiple-isotope analysis is an established practice for many
54 light element systems (e.g., O, Si, S), there exist robust theoretical derivations for determining mass laws. Drawing

55 upon this theory, I estimate b values for several relevant kinetic and equilibrium reactions using both simple approx-
 56 imations as well as more robust computational chemistry approaches. I then explore how overall expressed isotope
 57 effects and mass laws may deviate from those calculated for elementary reactions when incorporated into a complex
 58 (enzymatic) reaction network such as acetogenic lipid biosynthesis. Given these results, I estimate that fractionation
 59 during lipid biosynthesis can only explain ^{14}C age offsets up to ≈ 40 yr and conclude that biomarker radiocarbon results
 60 can be confidently interpreted to reflect aging in the environment. I briefly offer alternative explanations to interpret
 61 the data of Lane et al. (2021).

Table 1: Compilation of bulk leaf tissue and non-blank-corrected acetogenic lipid (n -alkane, n -alkanoic acid) $\delta^{13}\text{C}$ and $F^{14}\text{C}$ data from living plants, including calculated $^{13}\alpha$ values (calculated using Eq. 6) and mass-law b values (calculated using Eq. 7) that would be required to explain observed age offsets if they were driven purely by fractionation. References are: [1] = Lane et al. (2021), [2] = Eglinton et al. (1996).

Species	Compounds	$F^{14}\text{C}$		$\delta^{13}\text{C}$ (‰ VPDB)		$\ln(^{13}\alpha)$ $\times 1000$ ‰	b	Ref.
		bulk leaf	lipid	bulk leaf	lipid			
<i>L. styraciflua</i> L.	n -alkanes ^a	1.003 ± 0.003^b	0.868 ± 0.002	-31.4^c	-34.7^c	-3.4	44.5	1
<i>M. virginiana</i> L.	n -alkanes ^a	1.005^c	0.815 ± 0.002	-27.5^c	-31.3^c	-3.9	55.3	1
<i>Q. nigra</i> L.	n -alkanes ^a	1.003 ± 0.003^b	0.810 ± 0.007	-28.7^c	-30.4^c	-1.8	123.8	1
<i>Q. virginiana</i> Mill.	n -alkanes ^a	1.005^c	0.923 ± 0.002	-29.3^c	-32.7^c	-3.5	26.2	1
<i>A. stricta</i> Michx.	n -alkanes ^a	1.004^c	0.866 ± 0.002	-14.1^c	-25.2^c	-11.3	15.1	1
<i>D. sanguinalis</i> L.	n -alkanes ^a	1.000^c	0.937 ± 0.002	-29.8^c	-36.3^c	-6.7	11.6	1
<i>C. argentea</i>	$n\text{-C}_{31}$ alkane ^d	0.887 ± 0.010	0.816 ± 0.011	-23.9^c	-38.1^c	-14.7	7.7	2
<i>A. americana</i>	$n\text{-C}_{16:0+18:0}$ FA ^e	1.098 ± 0.007	0.990 ± 0.021	-14.8^c	-27.8 ± 0.5	-13.3	9.8	2

^aUrea-adducted apolar lipid extract with no further separation or purification procedures; see Lane et al. (2021) for details.

^bValue not reported; taken as average of all reported bulk leaf tissue values from Lane et al. (2021) ($\mu \pm 1\sigma$; $n = 4$).

^cNo uncertainty reported in original publication.

^dMass-weighted average of all reported replicates after preparatory column gas chromatography ($\mu \pm 1\sigma$; $n = 3$).

^eMass-weighted average of all individually reported $n\text{-C}_{16:0}$ and $n\text{-C}_{18:0}$ separated by preparatory column gas chromatography ($\mu \pm 1\sigma$; $n = 2$).

62 2. Theory and methods

63 2.1. Radiocarbon nomenclature and mass law calculations

64 I first define the nomenclature and mathematical relationships required to estimate mass laws. Following Stuiver
 65 and Polach (1977) and Reimer et al. (2004), radiocarbon activity is typically reported in “fraction modern” as

$$F^{14}\text{C} = \frac{A_{s,N}}{0.95 \times A_{Ox,N}}, \quad (1)$$

66 where $A = {}^{14}\text{C}/\text{C}$ is the ${}^{14}\text{C}$ activity, s refers to the sample, Ox refers to the Ox-I oxalic acid standard, N indicates that
 67 both activities are normalized for isotope fractionation, and the scalar 0.95 is added by convention. To be consistent
 68 with stable isotope nomenclature, I let $A \approx {}^{14}\text{R}$, where ${}^{14}\text{R} = {}^{14}\text{C}/{}^{12}\text{C}$ is the ${}^{14}\text{C}$ isotope ratio; this approximation
 69 is commonly applied and has a negligible impact on calculated radiocarbon ages (Fahrni et al., 2017). Then, by
 70 explicitly including the fractionation normalization of Reimer et al. (2004), Eq. 1 becomes

$$F^{14}\text{C} = \frac{{}^{14}\text{R}_s}{{}^{14}\text{R}_{Ox}} \left(\frac{0.975}{0.981} \right)^{b_{RL}} \left(\frac{{}^{13}\text{R}_{Ox}}{{}^{13}\text{R}_s} \right)^{b_{RL}}, \quad (2)$$

71 where b_{RL} is the reference line mass law; following Craig (1954), nearly all $F^{14}\text{C}$ values are reported using $b_{RL} = 2.0$.
 72 The first parenthetical term in Eq. 2 reflects the convention that the sample and Ox-I are corrected to $\delta^{13}\text{C} = -25 \text{‰}$
 73 and $\delta^{13}\text{C} = -19 \text{‰}$, respectively, where

$$\delta^{13}\text{C} = \left({}^{13}\text{R}/{}^{13}\text{R}_{VPDB} - 1 \right) \times 1000 \text{‰}, \quad (3)$$

74 ${}^{13}\text{R} = {}^{13}\text{C}/{}^{12}\text{C}$, VPDB is the Vienna Pee Dee Belemnite reference material, and ‰ indicates “permil” notation.
 75 Finally, radiocarbon age in conventional ${}^{14}\text{C}$ yr can be calculated as

$${}^{14}\text{C yr} = -8033 \ln(F^{14}\text{C}). \quad (4)$$

76 Following Eq. 2, it is apparent that ${}^{14}\text{C}$ age biases may arise from isotope fractionation if a given fractionation process
 77 is described by a mass law that deviates from $b_{RL} = 2.0$. Mass laws for any kinetic or equilibrium fractionation
 78 process can be calculated following the relationship (Southon, 2011; Young et al., 2002):

$$b_{p/r} = \frac{\ln({}^{14}\alpha_{p/r})}{\ln({}^{13}\alpha_{p/r})}, \quad (5)$$

79 where

$${}^*\alpha_{p/r} = \frac{{}^*\text{R}_p}{{}^*\text{R}_r} \quad (6)$$

80 is the fractionation factor, $*$ = 13 or 14 is the isotope of interest, “p” refers to the product compound, and “r” refers to
 81 the reactant compound. Fahrni et al. (2017) showed that the mass-law b value for any process can be determined so
 82 long as the product and reactant $F^{14}\text{C}$ and $\delta^{13}\text{C}$ values are known. That is, combining Eqs. 2, 5, and 6 yields

$$b_{p/r} = b_{RL} + \frac{\ln(F^{14}\text{C}_p) - \ln(F^{14}\text{C}_r)}{\ln({}^{13}\alpha_{p/r})}. \quad (7)$$

83 Finally, Eqs. 4 and 7 can be combined to yield the ${}^{14}\text{C}$ age offset due to fractionation:

$${}^{14}\text{C yr offset (product - reactant)} = -8033 \ln({}^{13}\alpha_{p/r}) (b_{p/r} - b_{RL}). \quad (8)$$

84 I use Eq. 7 and data reported in Table 2 of Lane et al. (2021) to estimate $b_{p/r}$ values that would be required if their
 85 ${}^{14}\text{C}$ offsets between bulk leaf tissue and n -alkanes were due to fractionation (Table 1). When bulk leaf tissue $F^{14}\text{C}$

86 is not reported (i.e., for the species *L. styraciflua* and *Q. nigra* L.), I assume $F^{14}\text{C} = 1.003 \pm 0.003$, the average of
 87 all reported values ($\mu \pm 1\sigma$; $n = 4$). I calculate $^{13}\alpha_{p/r}$ using reported $\delta^{13}\text{C}$ values determined by isotope ratio mass
 88 spectrometry rather than those measured by accelerator mass spectrometry (AMS). This is appropriate here because
 89 $F^{14}\text{C}$ is determined using concomitantly measured, AMS-derived ^{13}R and ^{14}R values (Eq. 2); any fractionation during
 90 AMS analysis is thus already accounted for (c.f., Fahrni et al., 2017). Similarly, I use Eq. 8 to calculate predicted
 91 fractionation age offsets for kinetic, equilibrium, and complex reaction network processes using all $^{13}\alpha_{p/r}$ and $b_{p/r}$
 92 estimates determined in this study.

Table 2: Estimated b^{kin} values calculated using Eq. 9 with $^x n = ^x M$ (i.e., ideal gas diffusion) and with $^x n = ^x \mu$ (i.e., bond breaking to form a transition state) for a suite of compounds relevant to acetogenic lipid biosynthesis.

Compound	^{12}M (amu)	b^{kin}	
		$^x n = ^x M$	$^x n = ^x \mu$
acetic acid	66.06	1.982	1.909
malonic acid	108.04	1.987	1.914
pyruvic acid	92.04	1.986	1.913
acetyl-ACP ^a	452.26	1.994	1.920
acetyl-CoA	847.36	1.995	1.921
malonyl-ACP ^a	469.25	1.994	1.921
malonyl-CoA	891.35	1.995	1.922
acetoacetyl-ACP ^a	469.29	1.994	1.921
Acetyl-ACP enolate ^a	423.25	1.994	1.920
<i>n</i> -C ₁₆ alkanolic acid	288.44	1.993	1.919
<i>n</i> -C ₃₂ alkanolic acid	544.89	1.995	1.921
mean \pm std. dev. ($n = 11$)		1.992 \pm 0.005	1.918 \pm 0.004

^aAcyl Carrier Protein, truncated at phosphopantetheine group.

93 2.2. Kinetic mass law estimates

94 Following Young et al. (2002), kinetic fractionation mass laws can be estimated using the general formula:

$$b^{kin} = \frac{\ln\left(\frac{^{12}n/^{14}n}{^{12}n/^{13}n}\right)}{\ln\left(\frac{^{12}n/^{13}n}{^{12}n/^{14}n}\right)}, \quad (9)$$

95 where $^x n$ is some measure of the mass of a molecule containing isotope x ; I have added the superscript *kin* to explicitly
 96 indicate these are kinetic b values. Equation 9 is derived from transition state theory (Bigeleisen, 1949); it ignores
 97 temperature dependence and assumes purely classical mechanics (although a similar relationship can be derived using
 98 Marcus theory for quantum bond vibrations; see Young et al., 2002). To explore the possible range of kinetic mass

99 laws associated with lipid biosynthesis, I apply Eq. 9 by calculating ${}^x n$ in two different ways: (i) ${}^x n = {}^x M$, the
 100 molecular mass of the compound of interest, and (ii) ${}^x n = {}^x \mu$, the reduced mass of the compound of interest,
 101 calculated as

$${}^x \mu = \frac{{}^x m M}{{}^x m + M}, \quad (10)$$

102 where ${}^x m$ is the atomic mass of a given carbon isotope (i.e., ${}^x m = 12, 13,$ or 14 amu) and M is the (isotopically
 103 unsubstituted) mass of all other atoms bonded to the atom of interest (i.e., $M = {}^x M - {}^x m$). Case (i) represents diffusion
 104 of an ideal gas, whereas case (ii) represents the breaking of a bond to form a transition state; these should roughly
 105 represent upper- and lower-bounds, respectively, for b^{kin} values (Young et al., 2002). I calculate b for both cases for
 106 suite of compounds relevant to lipid biosynthesis (acetic acid, malonic acid, pyruvic acid, acetyl-ACP, acetyl-CoA,
 107 malonyl-ACP, malonyl-CoA, acetoacetyl-ACP, acetyl-ACP enolate, n -C₁₆ and n -C₃₂ alkanolic acids); these compounds
 108 were chosen to span broad M range, and resulting b variability should therefore be conservative. For all calculations,
 109 I assume the only isotopic substitution occurs at the atom of interest. Resulting b^{kin} ranges are shown in Fig. 1 and
 110 individual values are reported in Table 2.

Table 3: Estimated ${}^*\beta$ values for a suite of compounds relevant to acetogenic lipid biosynthesis calculated using Eq. 12 and reported at several physiologically relevant temperatures

Compound	$\ln({}^{13}\beta) \times 1000$			$\ln({}^{14}\beta) \times 1000$		
	0 °C	25 °C	50 °C	0 °C	25 °C	50 °C
pyruvic acid	179.77	157.97	142.35	335.99	295.06	265.75
acetyl-ACP ^a	158.90	139.56	125.72	296.44	260.22	234.33
acetyl-CoA	160.05	140.55	126.61	298.62	262.11	236.02
malonyl-ACP ^a	180.14	157.84	141.90	336.59	294.75	264.86
malonyl-CoA	180.94	158.54	142.52	338.07	296.05	266.03
acetoacetyl-ACP ^a	167.80	147.13	132.35	313.08	274.39	246.75
Acetyl-ACP enolate ^a	145.08	127.34	114.67	270.84	237.60	213.86

^aAcyl Carrier Protein, truncated at phosphopantetheine group.

111 2.3. Equilibrium mass law estimates

112 The equilibrium mass law for the triple-carbon isotope system can be estimated as

$$b^{eq} = \frac{\frac{1}{{}^{12}m} - \frac{1}{{}^{14}m}}{\frac{1}{{}^{12}m} - \frac{1}{{}^{13}m}} = 1.854, \quad (11)$$

113 where I have similarly added the superscript eq to explicitly indicate equilibrium b values. This relationship is derived
 114 from the quantum vibrational modes of the reduced partition function ratio (RPFR) assuming a harmonic oscillator

115 (Bigeleisen and Goeppert Mayer, 1947; Urey, 1947); it is unique to a given isotope system and can be interpreted
 116 as the high-temperature limit of equilibrium fractionation between ideal, monoatomic atoms (Young et al., 2002).
 117 Still, equilibrium fractionation between any two compounds at temperatures relevant to Earth-surface conditions may
 118 deviate from this value. Although several steps of the acetogenic lipid biosynthesis pathway are unidirectional and
 119 irreversible (Wakil, 1989; Pearson, 2014), determining equilibrium mass laws between all relevant compounds may
 120 nonetheless provide a useful limit to explore the possible range of expressed b values. To provide robust constraints
 121 on this range, I estimate b^{eq} values using RPFs determined by density functional theory using the computational
 122 chemistry software Gaussian 16 (Frisch et al., 2016).

123 Briefly, RPFs for any isotopologue can be determined following the Bigeleisen-Goeppert Mayer-Urey equation
 124 (Bigeleisen and Goeppert Mayer, 1947; Urey, 1947):

$${}^*\beta(T) = \frac{s}{s^*} \prod_{i=1}^{3N-y} \frac{u_i^*(T)}{u_i(T)} \frac{e^{-u_i^*(T)/2}}{e^{-u_i(T)/2}} \frac{1 - e^{-u_i(T)}}{1 - e^{-u_i(T)^*}}, \quad (12)$$

125 where

$$u_i(T) = \frac{h\omega_i}{k_B T}, \quad (13)$$

126 h is Planck's constant, ω_i is the harmonic normal mode frequency for degree-of-freedom i , k_B is Boltzmann's constant,
 127 T is temperature in Kelvin, s is the rotational symmetry number, N is the number of atoms in the compound of interest,
 128 and $y = 5$ for linear molecules or $y = 6$ for nonlinear molecules. Here, ${}^*\beta$ is the RPF multiplied by the rotational
 129 symmetry number ratio (typically, $s/s^* = 1$ since isotopic substitution often does not change rotational symmetry).
 130 Following Cao and Liu (2011), equilibrium fractionation factors can be calculated as

$${}^*\alpha_{p/r}^{eq} = \frac{{}^*\beta_p}{{}^*\beta_r}, \quad (14)$$

131 and b^{eq} values can then determined following Eq. 5.

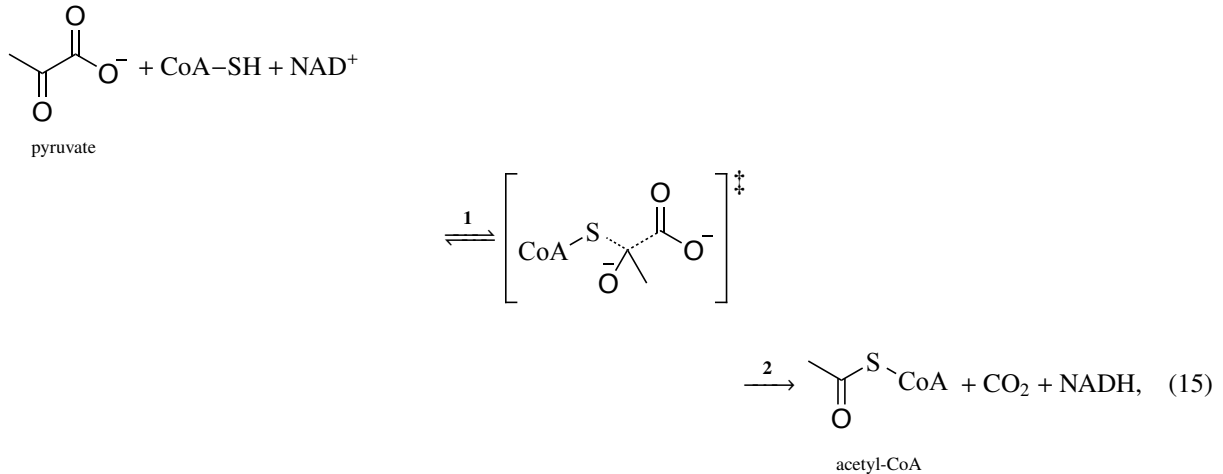
132 Here, I determine ω_i values and calculate ${}^*\beta(T)$ for a suite of compounds relevant to lipid biosynthesis (acetyl-ACP,
 133 acetyl-CoA, malonyl-ACP, malonyl-CoA, acetoacetyl-ACP, acetyl-ACP enolate, pyruvic acid) using the B3LYP/6-
 134 31G(d) method and basis set (Lee et al., 1988; Francl et al., 1982). This method and basis set were chosen as a
 135 balance between accuracy and computational efficiency; they are a common choice for triple-isotope studies (e.g.,
 136 Cao and Liu, 2011). All compound geometries were optimized in H₂O solvent using the C-PCM solvation method
 137 (Barone and Cossi, 1998); for all analyses, stationary points were found and no imaginary frequencies were observed,
 138 indicating proper convergence.

139 Reported ${}^*\beta(T)$ values represent the average of results calculated for single isotope substitutions at all relevant
 140 carbon positions (e.g., at the C1 and C2 positions of acetate-containing compounds), assuming all other atoms in the
 141 molecule are isotopically unsubstituted. This practice dampens the influence of any small geometric perturbations
 142 that may spuriously influence ω_i values; however, it yields results that cannot discern between site-specific isotope
 143 compositions such as the odd-over-even C position pattern observed by Monson and Hayes (1982). No attempt was

144 made to correct for anharmonic effects or computational basis-set scaling factors. These corrections may influence
 145 calculated $^{13}\alpha$ by several permil, but they have been shown to negligibly impact triple-isotope mass laws to due error
 146 cancellation (Cao and Liu, 2011). I therefore assume calculated b^{eq} values are robust. Results are shown in Fig. 1 and
 147 $^*\beta$ values are reported in Table 3 at several physiologically relevant temperatures.

148 2.4. Expressed mass laws for complex reaction networks

Finally, I explore the range of possible mass laws—and thus ^{14}C age offsets—that can be expressed by multi-step reaction networks. For example, consider the enzymatic decarboxylation of pyruvate by the pyruvate dehydrogenase complex to form acetyl-CoA, the building block for all acetogenic lipids (Pearson, 2014). This reaction has been shown to yield product acetyl-CoA that is depleted in ^{13}C relative to reactant pyruvate; it has thus been invoked to explain observed *n*-alkanoic acid ^{13}C depletion relative to bulk biomass (Monson and Hayes, 1982). Although the overall reaction is unidirectional and irreversible, for the purpose of predicting isotope fractionation factors it is useful to consider the reversible formation of a transition state (e.g., Bigeleisen, 1949; Bao et al., 2015). The reaction can then be written as



149 where \ddagger represents the transition state. Equation 15 is a specific case of the general reaction network:



150 where r is a reactant, t is a transition state, and p is a product. For a network of this form, Wing and Halevy (2014)
 151 showed that the net expressed fractionation factor can be written as

$$^{13}\alpha_{p/r}^{net} = \left(^{13}\alpha_2^k \times ^{13}\alpha_1^{eq} - ^{13}\alpha_1^k \right) \times f + ^{13}\alpha_1^k, \quad (17)$$

152 where subscripts 1 and 2 refer to the reaction steps in Eq. 15, superscripts k and eq refer to equilibrium or kinetic
 153 fractionation factors, and f reflects the degree to which reaction step 1 is reversible (i.e., the backward to forward flux
 154 ratio). Equation 17 can be similarly written for $^{14}\alpha_{p/r}^{net}$ in terms of step-specific $^{13}\alpha$ and b values; the overall expressed

155 mass law, $b_{p/r}^{net}$, is then determined following Eq. 5. Several other lipid biosynthesis steps can be interpreted using a
156 reaction pathway analogous to Eq. 16.

157 To investigate ^{14}C age offsets during acetyl-CoA formation, I solve Eq. 17 using a Monte Carlo approach. Specif-
158 ically, I draw all input variables from uniform distributions assuming: $^{13}\alpha_1^k \in (0.985, 1.000)$, $^{13}\alpha_2^k \in (0.985, 1.000)$,
159 $^{13}\alpha_1^{eq} \in (0.980, 1.020)$, $b_1^k \in (1.85, 2.00)$, $b_2^k \in (1.80, 2.00)$, $b_1^{eq} \in (1.86, 1.88)$, and $f \in (0, 1)$. These ranges were
160 chosen for the following reasons: (i) kinetic $^{13}\alpha$ values for both steps encompass all observed plant-wax lipid frac-
161 tionation factors in Chikaraishi et al. (2004), (ii) kinetic b values span the entire canonical range (Fig. 1; Stern and
162 Vogel, 1971), (iii) equilibrium $^{13}\alpha$ and b values encompass the range calculated in Section 2.3 for all reaction pairs
163 (Fig. 1), (iv) f spans the entire range from purely kinetic (unidirectional) to purely equilibrium (equal backward and
164 forward fluxes). Resulting $^{13}\alpha_{p/r}^{net}$, $b_{p/r}^{net}$, and ^{14}C age offset ranges are therefore expected to be conservative estimates;
165 true ranges are likely to be much narrower, particularly for $^{13}\alpha_{p/r}^{net}$ (e.g., Chikaraishi et al., 2004). Results for $n = 5000$
166 Monte Carlo draws are shown in Fig. 2.

167 3. Results and discussion

168 3.1. Predicted mass laws and age offsets

169 All kinetic b values calculated here fall within the canonical range, from a minimum of 1.909 to a maximum
170 of 1.995 (Fig. 1; Table 2). Importantly, this includes predictions both for ideal gas molecular diffusion (calculated
171 using molecular masses) and for bond breaking (calculated using reduced masses) for a suite of compounds ranging
172 in size from acetic acid (66 amu) to malonyl-CoA (891 amu). In general, b predictions for diffusion (1.992 ± 0.005)
173 are higher than those for bond breaking (1.918 ± 0.004). Although I do not expect any compounds involved in lipid
174 biosynthesis to follow ideal gas diffusive behavior, it is nonetheless a useful limiting case to estimate maximum b^{kin}
175 values. The observation that molecular diffusion approaches the reference line value ($b_{RL} = 2.0$) is consistent with a
176 previously measured triple-oxygen mass law for O_2 diffusion of $b = 1.978$ (Yeung et al., 2012). Similarly, predicted
177 b^{kin} values for bond breaking and transition-state formation are consistent with previous estimates for several abiotic
178 S_N1 , S_N2 , E2, hydrogen transfer, and decarboxylation reactions (Stern and Vogel, 1971; Bigeleisen and Wolfsberg,
179 1953; Bigeleisen, 1952), as well as triple-oxygen and triple-sulfur kinetic mass laws expressed for several metabolic
180 pathways (e.g., Wing and Halevy, 2014; Ash et al., 2020). Interestingly, measured mass laws for photosynthesis
181 (1.953 ± 0.025 ; Fahrni et al., 2017) lie between the diffusion and bond-breaking scenarios calculated here, possibly
182 reflecting the importance of CO_2 diffusion relative to that of isotope fractionation imparted by the RuBisCo enzyme
183 (O'Leary, 1981). In general, I conclude that mass laws for all kinetic processes should lie within the canonical range.

184 Similarly, equilibrium b values calculated here for a suite of steps involved in acetogenic lipid biosynthesis all
185 fall within a narrow range of 1.854 to 1.895 and exhibit only a small dependence on temperature (Fig. 1; Table
186 3). Although several of these steps are unidirectional and are thus not expected to operate in equilibrium in nature,
187 these results again represent a useful limiting case to estimate minimum b values. For all studied reactions, $b_{p/r}^{eq}$

188 approaches the high-temperature, mono-atomic limit of $b = 1.854$ and is consistently lower than any calculated b^{kin}
 189 value. Computational chemistry results also yield $^{13}\alpha_{p/r}^{eq}$ estimates (Fig. 1A), allowing one to predict the ^{14}C age
 190 offsets that would be imparted by these reactions (Eq. 8). In all cases, equilibrium isotope fractionation leads to a
 191 maximum age offset of ≈ 30 ^{14}C yr (Fig. 1C) despite the large range in predicted $^{13}\alpha_{p/r}^{eq}$ values. This result confirms
 192 previous observations that small differences between measured b and b_{RL} will lead to small ^{14}C age biases even if $^{13}\alpha$
 193 is large (Stuiver and Robinson, 1974; Southon, 2011; Fahrni et al., 2017). Similar to the b^{kin} case, I conclude that all
 194 equilibrium fractionation processes should lie within the canonical b range and that resulting ^{14}C age biases should be
 195 negligible.

196 In contrast to all b^{kin} and $b_{p/r}^{eq}$ predictions, b^{net} values for multi-step reaction networks may reach non-canonical
 197 values much higher than 2.0 (Fig. 2C). However, Eq. 5 shows that non-canonical b values only manifest in the limiting
 198 case that $\ln(^{13}\alpha_{p/r}^{net}) \rightarrow 0$. For the simplified reaction network here (Eq. 15) this occurs when

$$^{13}\alpha_1^{eq} \approx \frac{1 - ^{13}\alpha_1^k(1-f)}{^{13}\alpha_2^k f}, \quad (18)$$

199 which can be accomplished either when $f = 0$ and $^{13}\alpha_1^k = 1.0$ or when $f \neq 0$ and $^{13}\alpha_1^{eq} > 1.0$ (assuming $^{13}\alpha_1^k$
 200 and $^{13}\alpha_2^k < 1.0$). In general, large b^{net} values can manifest at so-called ‘‘crossover’’ points when one step of a reaction
 201 network is described by $^{13}\alpha > 1$ while another is described by $^{13}\alpha < 1$; this phenomenon has been observed previously
 202 both for triple-carbon and for triple-oxygen mass laws (Stern and Vogel, 1971; Bao et al., 2015). However, despite
 203 the potential for large b^{net} values, crossover points will not yield large ^{14}C age offsets since $\ln(^{13}\alpha) \rightarrow 0$ (Eq. 8). That
 204 is, this large, non-canonical mass law is not expressed because carbon is not being isotopically fractionated. This can
 205 be seen in Fig. 2B, which shows that ^{14}C age offsets are always within $\approx \pm 40$ yr despite the large, conservative input
 206 parameter range and the possibility of crossover points.

207 Interestingly, this phenomenon may explain the one reliable documented experimental case that yielded $b > 2.0$ —
 208 the two-step enzymatic hydrolysis of urea ($b = 3.17 \pm 0.38$; Schmitt et al., 1952). Several other experiments have
 209 reported $b > 2.0$, but these have largely been discredited as experimental artifacts (e.g., Southon, 2011); in contrast,
 210 the urea hydrolysis results are thought to be robust (Stern and Vogel, 1971). This reaction is known to follow a two-
 211 step pathway with a transition-state intermediate similar to the network shown in Eq. 16. If the corresponding $^{13}\alpha^{net}$
 212 is sufficiently close to 1.0, then the observed b value could be the result of a crossover point. Other than this reaction,
 213 I know of no other biological process that has been reliably documented to yield triple-isotope mass laws outside of
 214 the canonical, mass-dependent range.

215 3.2. Are large biosynthetic ^{14}C age biases possible?

216 Given the range of kinetic, equilibrium, and net reaction mass laws observed here, it is possible to assess the
 217 claim made by Lane et al. (2021) that biosynthetic fractionation imparts ^{14}C age biases up to ≈ 1500 yr. In contrast
 218 to the large mass laws required for this hypothesis, I find that b values for all investigated kinetic and equilibrium
 219 fractionation process are within the canonical range of 1.8 to 2.0 (Fig. 1; Tables 2–3). Similarly, I show that large

220 expressed b values in multi-step reaction networks are only possible when overall fractionation trends to zero, thus
221 imparting no appreciable age offset (Fig. 2). This finding is consistent with all literature mass-laws for biological and
222 chemical processes for carbon, oxygen, and sulfur triple-oxygen isotope systems. Even when including experimental
223 results that were subsequently disproven as artifacts (see e.g., Southon, 2011), I am unaware of any literature b value
224 for the triple-carbon isotope system above ≈ 5 (Stern and Vogel, 1971); this is $\approx 2\times$ lower than the minimum value
225 and $\approx 60\times$ lower than the maximum value required to explain the results of Lane et al. (2021). In contrast, so-called
226 “mass-independent” fractionation—which has been observed in the triple-oxygen and triple-sulfur isotope systems—
227 would lead to $b \approx 1.0$ (e.g., Thiemens and Lin, 2021). Still, this phenomenon is limited to gas-phase species in which
228 an isotope substitution imparts asymmetry, which doubles the accessible rotational states compared to the symmetric
229 isotopologue (Thiemens and Lin, 2021; Young et al., 2002). This is not the case for the reactions considered here.
230 I thus conclude that b values for all steps during lipid biosynthesis fall within the canonical range and that isotope
231 fractionation cannot explain large apparent ^{14}C age offsets.

232 Furthermore, Lane et al. (2021) hypothesize that differences in observed ^{14}C age offsets imply species-specific
233 biosynthetic mass laws, further complicating the interpretation of biomarker ^{14}C ages. However, this interpretation
234 would require an unprecedented level of biosynthetic mass-law variability, particularly between species within the C_3
235 angiosperms (b ranging from 26.2 to 123.8; Table 1). Even if b values as high as 123.8 were possible, this species-
236 specific variability is highly suspect for several reasons.

237 First, although many proteins are involved in the overall biosynthesis of acetogenic lipids, several steps occur
238 in different subunits of the multi-enzyme fatty acid synthase protein, which is highly conserved (Wakil, 1989). In
239 particular, the amino acid sequences involved in the ester binding of acetyl and malonyl groups exhibit high homology
240 across multiple domains of life (Yang et al., 1988; Wakil, 1989); these (reversible) binding steps ensure substrate entry
241 into the subsequent synthesis cascade. Such high sequence homology therefore implies that this critical step of the
242 biosynthetic pathway will exhibit similar active-site structure and thus similar fractionation factors and mass laws
243 across all species.

244 Second, even if fatty acid synthase active sites between species are variable—or if a different, less conserved
245 enzyme imparts the observed isotope fractionation—the range of b values invoked here is inconsistent with inter-
246 species net mass-law variability observed for other multiple-isotope systems. For example, Wing and Halevy (2014)
247 observe $^{33}\lambda$ values ranging from 0.506 to 0.516 (equivalent to $b = 1.94$ to 1.98 in the nomenclature used here) for
248 different sulfate reducing bacteria under different nutrient conditions, even as $^{34}\alpha$ values exhibit large variability.
249 Similarly, Ash et al. (2020) describe $^{17}\theta$ values between 0.523 and 0.525 (equivalent to $b = 1.90$ to 1.91) for different
250 O_2 -binding enzymes involved in oxic respiration. In addition to being within the canonical mass-law ranges for triple-
251 sulfur and triple-oxygen isotope fractionation, observed variability in both of these studies is three orders of magnitude
252 smaller than the range in species-specific b values invoked by Lane et al. (2021).

253 Finally, large b variability may be possible at the $^{13}\alpha$ crossover point; however, all ^{13}C fractionations reported
254 in Lane et al. (2021) are far from this point (Fig. 2). Although the reaction network used here is highly simplified,

255 solutions to Eq. 15 suggests that b cannot exceed ≈ 2.4 within the observed $^{13}\alpha_{\text{lipid/leaf}}$ range (Fig. 2C). A more
256 complicated reaction network is unlikely to invalidate this result. Interestingly, Chikaraishi et al. (2004) do observe
257 C_3 angiosperms with n -alkanoic acid $\delta^{13}\text{C}$ values similar to—or slightly higher than—bulk leaf tissue $\delta^{13}\text{C}$, suggest-
258 ing that acetogenic lipid biosynthesis near the crossover point may be possible. Nonetheless, I emphasize that this
259 phenomenon will not impart an appreciable ^{14}C age offset since $\ln(^{13}\alpha) \rightarrow 0$ at the crossover point (Eq. 8; Fig. 2B).

260 Thus, the claim that different plant species will biosynthesize acetogenic lipids following highly variable b values
261 is inconsistent with the known biochemistry of fatty acid production, enzymatic isotope fractionations, and all other
262 observed biological mass laws—with a possible exception at the ^{13}C crossover point, where no ^{14}C age offset is
263 expressed.

264 3.3. Interpreting anomalously old ^{14}C ages

265 Because biosynthetic fractionation cannot explain the anomalously old ^{14}C ages observed in Lane et al. (2021), this
266 result must instead reflect incorporation of ^{14}C -depleted contaminant carbon. Similar biomarker age offsets have been
267 observed previously and have been interpreted to reflect contamination by petrochemicals such as gas chromatography
268 column bleed, residual solvent, urea, etc., during sample preparation (Table 1; Eglinton et al., 1996; Cisneros-Dozal
269 et al., 2016). Many of these contaminants are removed by preparatory-column gas chromatography, which is typically
270 utilized when isolating individual compounds for ^{14}C analysis (Eglinton et al., 1996); however, this method was not
271 employed by Lane et al. (2021). Interestingly, Lane et al. (2021) considered but ultimately dismissed possibility that
272 their results reflect ^{14}C -depleted blank contributions since their sample preparation procedure was careful to avoid
273 possible contamination steps. However, no thorough blank assessment was performed. For example, previous blank
274 assessment studies using the “modern-dead” isotope dilution approach—in which deviations from accepted $F^{14}\text{C}$
275 values for a suite of known standards are measured—have revealed large and variable contaminations, particularly for
276 small samples and individual compounds (Santos et al., 2010). A similar blank assessment for the sample preparation
277 procedure used in Lane et al. (2021) would be highly informative.

278 One plausible alternative explanation may be fossil-fuel derived deposition. Although Lane et al. (2021) were
279 careful to avoid sampling near population centers, their sample site is ≈ 40 km from the 1600 MW coal-fired Weather-
280 spoon Power Plant, which is known to emit aerosols via cooling towers (USDOE, 2007). Aerosol deposition on plant
281 leaves is well documented (Wedding et al., 1975); if deposited aerosols are rich in apolar and aliphatic compounds,
282 then this deposition may survive aqueous cleaning steps and impact the extracted n -alkanes while having a minor or
283 negligible impact on bulk leaf tissue ^{14}C ages. Still, this explanation remains speculative.

284 4. Conclusions and outlook

285 Simple mass-law approximations and computational chemistry results indicate that each investigated step of the
286 n -alkanoic acid biosynthetic pathway is described by canonical kinetic and equilibrium b values between 1.8 and 2.0,

287 consistent with all previously reported biological and chemical processes (e.g., Fahrni et al., 2017; Southon, 2011;
288 Bigeleisen and Wolfsberg, 1953; Bigeleisen, 1949; Stern and Vogel, 1971). Using a simplified reaction network,
289 I show theoretically that non-canonical b values can be expressed for multi-step (enzymatic) reactions such as n -
290 alkanolic acid biosynthesis, but only at “crossover” points when $\ln(^{13}\alpha_{p/r}^{net}) \rightarrow 0$. This behavior has been shown
291 previously for several isotope systems (Stern and Vogel, 1971; Bao et al., 2015), and it may explain the only reliable,
292 experimentally determined, non-canonical ^{14}C mass law reported in the literature—the two-step enzymatic hydrolysis
293 of urea ($b = 3.17 \pm 0.38$; Schmitt et al., 1952). Because large b requires $\ln(^{13}\alpha_{p/r}^{net}) \approx 0$, fractionation leads to maximum
294 ^{14}C age offsets on the order of decades, similar to the ^{14}C analytical uncertainty. I therefore conclude that biomarker
295 ^{14}C ages are robust to isotope fractionation during biosynthesis and that they can be confidently interpreted as a tracer
296 for storage and turnover time in the environment after proper blank correction.

297 Acknowledgements

298 I thank Kevin Sutherland, Valier Galy, Ann McNichol, Tim Eglinton, Rienk Smittenberg, and the WHOI and ETH
299 Radiocarbon Reading Groups for helpful and thought-provoking discussions related to this topic. The computations
300 in this paper were run on the FASRC Cannon cluster supported by the FAS Division of Science Research Computing
301 Group at Harvard University. No funding was provided for this work.

302 References

- 303 Ash, J.L., Hu, H., Yeung, L.Y., 2020. What fractionates oxygen isotopes during respiration? insights from multiple isotopologue measurements
304 and theory. *ACS Earth and Space Chemistry* 4, 50–66.
- 305 Bao, H., Cao, X., Hayles, J.A., 2015. The confines of triple oxygen isotope exponents in elemental and complex mass-dependent processes.
306 *Geochimica et Cosmochimica Acta* 170, 39–50.
- 307 Barone, V., Cossi, M., 1998. Quantum calculation of molecular energies and energy gradients in solution by a conductor solvent model. *Journal of*
308 *Physical Chemistry A* 102, 1995–2001.
- 309 Bigeleisen, J., 1949. The relative reaction velocities of isotopic molecules. *Journal of Chemical Physics* 17, 675–678.
- 310 Bigeleisen, J., 1952. The effects of isotopic substitution on the rates of chemical reactions. *Journal of Physical Chemistry* 56, 823–828.
- 311 Bigeleisen, J., Goepfert Mayer, M., 1947. Calculation of equilibrium constants for isotopic exchange reactions. *Journal of Chemical Physics* 15,
312 261–267.
- 313 Bigeleisen, J., Wolfsberg, M., 1953. Fractionation of the carbon isotopes in decarboxylation reactions. VI. Comparison of the intermolecular
314 isotope effects of a pair of isotopic isomers. *Journal of Chemical Physics* 21, 2120–2121.
- 315 Cao, X., Liu, Y., 2011. Equilibrium mass-dependent fractionation relationships for triple oxygen isotopes. *Geochimica et Cosmochimica Acta* 75,
316 7435–7445.
- 317 Chikaraishi, Y., Naraoka, H., Poulson, S.R., 2004. Hydrogen and carbon isotopic fractionations of lipid biosynthesis among terrestrial (C3, C4 and
318 CAM) and aquatic plants. *Phytochemistry* 65, 1369–1381.
- 319 Cisneros-Dozal, L., Xu, X., Bryant, C., Pearson, E., Dungait, J., 2016. Grass material as a modern process standard for ^{14}C analysis of n -alkanes.
320 *Radiocarbon* 58, 445–458.
- 321 Coppola, A.I., Wiedemeier, D.B., Galy, V., Hagepour, N., Hanke, U.M., Nascimento, G.S., Usman, M., Blattmann, T.M., Reisser, M., Freymond,
322 C.V., Zhao, M., Voss, B., Wacker, L., Schefuß, E., Peucker-Ehrenbrink, B., Abiven, S., Schmidt, M.W., Eglinton, T.I., 2018. Global-scale
323 evidence for the refractory nature of riverine black carbon. *Nature Geoscience* 11, 584–588.

324 Craig, H., 1954. Carbon 13 in plants and the relationships between carbon 13 and carbon 14 variations in nature. *Journal of Geology* 62, 115–149.

325 Eglinton, T.I., Aluwihare, L.I., Bauer, J.E., Druffel, E.R., McNichol, A.P., 1996. Gas chromatographic isolation of individual compounds from
326 complex matrices for radiocarbon dating. *Analytical Chemistry* 68, 904–912.

327 Eglinton, T.I., Benitez-Nelson, B.C., Pearson, A., McNichol, A.P., Bauer, J.E., Druffel, E.R., 1997. Variability in radiocarbon ages of individual
328 organic compounds from marine sediments. *Science* 277, 796–799.

329 Eglinton, T.I., Galy, V.V., Hemingway, J.D., Feng, X., Bao, H., Blattmann, T.M., Dickens, A.F., Gies, H., Giosan, L., Haghypour, N., Hou, P.,
330 Lupker, M., McIntyre, C.P., Montluçon, D.B., Peucker-Ehrenbrink, B., Ponton, C., Schefuß, E., Schwab, M.S., Voss, B.M., Wacker, L., Wu, Y.,
331 Zhao, M., 2021. Climate control on terrestrial biospheric carbon turnover. *Proceedings of the National Academy of Sciences* 118, e2011585118.

332 Farni, S.M., Southon, J.R., Santos, G.M., Palstra, S.W., Meijer, H.A., Xu, X., 2017. Reassessment of the $^{13}\text{C}/^{12}\text{C}$ and $^{14}\text{C}/^{12}\text{C}$ isotopic
333 fractionation ratio and its impact on high-precision radiocarbon dating. *Geochimica et Cosmochimica Acta* 213, 330–345.

334 Feng, X., Vonk, J.E., van Dongen, B.E., Gustafsson, Ö., Semiletov, I.P., Dudarev, O.V., Wang, S., Montluçon, D.B., Wacker, L., Eglinton, T.I.,
335 2013. Differential mobilization of terrestrial carbon pools in Eurasian Arctic river basins. *Proceedings of the National Academy of Sciences*
336 110, 14168–14173.

337 Francl, M.M., Pietro, W.J., Hehre, W.J., Binkley, J.S., Gordon, M.S., DeFrees, D.J., Pople, J.A., 1982. Self-consistent molecular orbital methods.
338 XXIII. A polarization-type basis set for second-row elements. *Journal of Chemical Physics* 77, 3654–3665.

339 Frisch, M.J., Trucks, G.W., Schlegel, H.B., Scuseria, G.E., Robb, M.A., Cheeseman, J.R., Scalmani, G., Barone, V., Petersson, G.A., Nakatsuji,
340 H., Li, X., Caricato, M., Marenich, A.V., Bloino, J., Janesko, B.G., Gomperts, R., Mennucci, B., Hratchian, H.P., Ortiz, J.V., Izmaylov, A.F.,
341 Sonnenberg, J.L., Williams-Young, D., Ding, F., Lipparini, F., Egidi, F., Goings, J., Peng, B., Petrone, A., Henderson, T., Ranasinghe, D.,
342 Zakrzewski, V.G., Gao, J., Rega, N., Zheng, G., Liang, W., Hada, M., Ehara, M., Toyota, K., Fukuda, R., Hasegawa, J., Ishida, M., Nakajima, T.,
343 Honda, Y., Kitao, O., Nakai, H., Vreven, T., Throssell, K., Montgomery, Jr., J.A., Peralta, J.E., Ogliaro, F., Bearpark, M.J., Heyd, J.J., Brothers,
344 E.N., Kudin, K.N., Staroverov, V.N., Keith, T.A., Kobayashi, R., Normand, J., Raghavachari, K., Rendell, A.P., Burant, J.C., Iyengar, S.S.,
345 Tomasi, J., Cossi, M., Millam, J.M., Klene, M., Adamo, C., Cammi, R., Ochterski, J.W., Martin, R.L., Morokuma, K., Farkas, O., Foresman,
346 J.B., Fox, D.J., 2016. Gaussian 16 Revision C.01. Gaussian Inc. Wallingford CT.

347 Hein, C.J., Usman, M., Eglinton, T.I., Haghypour, N., Galy, V.V., 2020. Millennial-scale hydroclimate controls of tropical soil carbon storage.
348 *Nature* 581, 63–66.

349 Hemingway, J.D., Hilton, R.G., Hovius, N., Eglinton, T.I., Haghypour, N., Wacker, L., Chen, M.C., Galy, V.V., 2018. Microbial oxidation of
350 lithospheric organic carbon in rapidly eroding tropical mountain soils. *Science* 360, 209–212.

351 Ingalls, A.E., Shah, S.R., Hansman, R.L., Aluwihare, L.I., Santos, G.M., Druffel, E.R., Pearson, A., 2006. Quantifying archaeal community
352 autotrophy in the mesopelagic ocean using natural radiocarbon. *Proceedings of the National Academy of Sciences* 103, 6442–6447.

353 Lane, C.S., Yanuskiewicz, E.A., Mead, R.N., Horn, S.P., 2021. Anomalously low radiocarbon content of modern *n*-alkanes. *Organic Geochemistry*
354 152, 104170.

355 Lee, C., Yang, W., Parr, R.G., 1988. Development of the Colle-Salvetti correlation-energy formula into a functional of the electron density. *Physical*
356 *Review B* 37, 785–789.

357 Monson, K.D., Hayes, J.M., 1982. Carbon isotopic fractionation in the biosynthesis of bacterial fatty acids. Ozonolysis of unsaturated fatty acids
358 as a means of determining the intramolecular distribution of carbon isotopes. *Geochimica et Cosmochimica Acta* 46, 139–149.

359 O’Leary, M.H., 1981. Carbon isotope fractionation in plants. *Phytochemistry* 20, 553–567.

360 Pearson, A., 2014. Lipidomics for geochemistry. *Treatise on Geochemistry* 12, 291–336.

361 Pearson, A., Eglinton, T.I., 2000. The origin of *n*-alkanes in Santa Monica Basin surface sediment: a model based on compound-specific $\Delta^{14}\text{C}$ and
362 $\delta^{13}\text{C}$ data. *Organic Geochemistry* 31, 1103–1116.

363 Petsch, S.T., Eglinton, T.I., Edwards, K.J., 2001. ^{14}C -dead living biomass: evidence for microbial assimilation of ancient organic carbon during
364 shale weathering. *Science* 292, 1127–1131.

365 Reimer, P.J., Brown, T.A., Reimer, R.W., 2004. Discussion: reporting and calibration of post-bomb ^{14}C data. *Radiocarbon* 46, 1299–1304.

366 Santos, G.M., Southon, J.R., Drenzek, N.J., Ziolkowski, L.A., Druffel, E., Xu, X., Zhang, D., Trumbore, S., Eglinton, T.I., Hughen, K.A., 2010.

367 Blank assessment for ultra-small radiocarbon samples: chemical extraction and separation versus AMS. *Radiocarbon* 52, 1322–1335.

368 Schmitt, J.A., Myerson, A.L., Daniels, F., 1952. Relative rates of hydrolysis of urea containing C¹⁴, C¹³, and C¹². *Journal of Physical Chemistry*

369 56, 917–920.

370 Smittenberg, R.H., Eglinton, T.I., Schouten, S., Sinninghe Damsté, J.S., 2006. Ongoing buildup of refractory organic carbon in boreal soils during

371 the Holocene. *Science* 314, 1283–1286.

372 Southon, J., 2011. Are the fractionation corrections correct: are the isotopic shifts for ¹⁴C/¹²C ratios in physical processes and chemical reactions

373 really twice those for ¹³C/¹²C? *Radiocarbon* 53, 691–704.

374 Steier, P., Dellinger, F., Kutschera, W., Priller, A., Rom, W., Wild, E.M., 2004. Pushing the precision limit of ¹⁴C AMS. *Radiocarbon* 46, 5–16.

375 Stern, M.J., Vogel, P.C., 1971. Relative ¹⁴C–¹³C kinetic isotope effects. *Journal of Chemical Physics* 55, 2007–2013.

376 Stuiver, M., Polach, H.A., 1977. Discussion: Reporting of ¹⁴C data. *Radiocarbon* 19, 355–363.

377 Stuiver, M., Robinson, S.W., 1974. University of Washington Geosecs North Atlantic carbon-14 results. *Earth and Planetary Science Letters* 23,

378 87–90.

379 Thiemens, M.H., Lin, M., 2021. Discoveries of mass independent isotope effects in the solar system: past, present, and future. *Reviews in*

380 *Mineralogy & Geochemistry* 86, 35–95.

381 Urey, H.C., 1947. The thermodynamic properties of isotopic substances. *Journal of the Chemical Society*, 562–581.

382 USDOE, 2007. The National Energy Technology Laboratory 2007 coal power plant database. Technical Report. United States Department of

383 Energy.

384 Wakil, S.J., 1989. Fatty acid synthase, a proficient multifunctional enzyme. *Biochemistry* 28, 4523–4530.

385 Wedding, J.B., Carlson, R.W., Stukel, J.J., Bazzaz, F., 1975. Aerosol deposition on plant leaves. *Environmental Science & Technology* 9, 151–153.

386 Wigley, T., Muller, A., 1981. Fractionation corrections in radiocarbon dating. *Radiocarbon* 23, 173–190.

387 Wing, B.A., Halevy, I., 2014. Intracellular metabolite levels shape sulfur isotope fractionation during microbial sulfate reduction. *Proceedings of*

388 *the National Academy of Sciences* 111, 18116–18125.

389 Yang, C.Y., Huang, W.Y., Chirala, S., Wakil, S.J., 1988. Complete amino acid sequence of the thioesterase domain of chicken liver fatty acid

390 synthase. *Biochemistry* 27, 7773–7777.

391 Yeung, L.Y., Young, E.D., Schauble, E.A., 2012. Measurements of ¹⁸O¹⁸O and ¹⁷O¹⁸O in the atmosphere and the role of isotope-exchange

392 reactions. *Journal of Geophysical Research* 117, D18306.

393 Young, E.D., Galy, A., Nagahara, H., 2002. Kinetic and equilibrium mass-dependent isotope fractionation laws in nature and their geochemical

394 and cosmochemical significance. *Geochimica et Cosmochimica Acta* 66, 1095–1104.

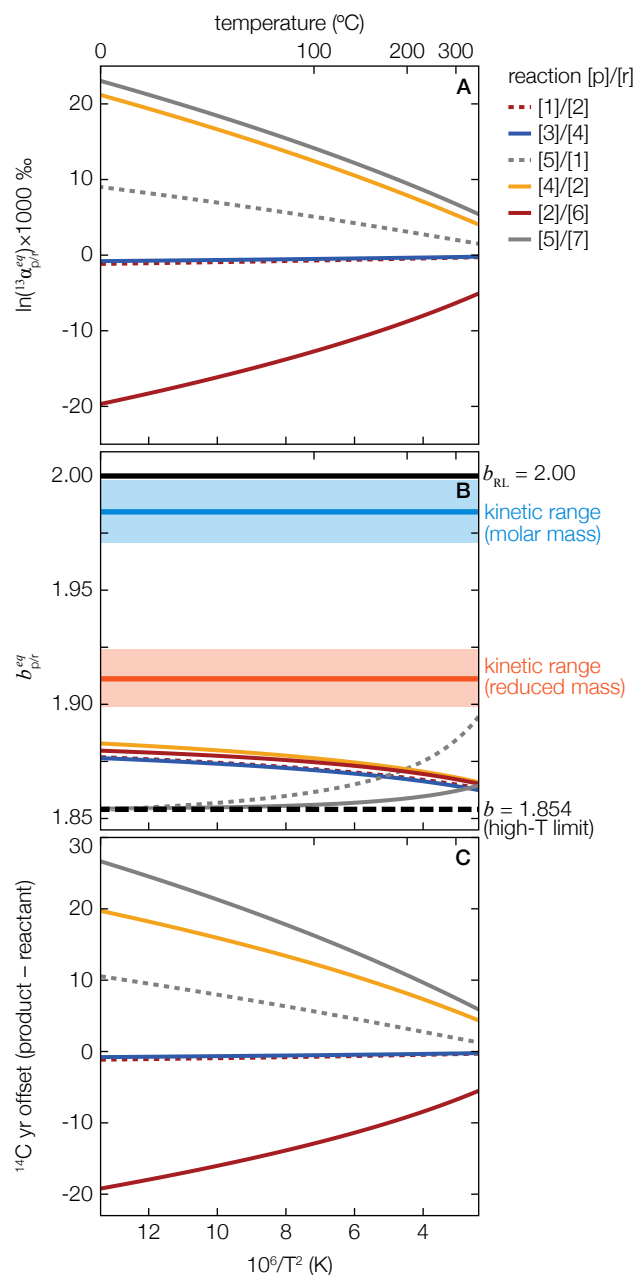


Figure 1: Calculated isotope effects. (A) $^{13}\alpha_{p/r}^{eq}$, (B) $b_{p/r}^{eq}$, and (C) ^{14}C age offsets for a suite of equilibrium reactions involving product (p) and reactant (r) compounds relevant for acetogenic lipid biosynthesis plotted as a function of reaction temperature. Compound numbers refer to: [1] = acetyl-ACP, [2] = acetyl-CoA, [3] = malonyl-ACP, [4] = malonyl-CoA, [5] = acetoacetyl-ACP, [6] = pyruvic acid, [7] = acetyl-ACP enolate, where CoA = coenzyme-A and ACP = acyl carrier protein (truncated at the phosphopantetheine group). Also shown in (B) are the predicted ranges of kinetic b values for all compounds reported in Table 2 ($\mu \pm 1\sigma$, $n = 11$) calculated using either their molar masses (i.e., diffusive processes) or their reduced masses (i.e., bond-breaking processes), as well as the high-temperature monoatomic equilibrium limit ($b = 1.854$) and the reference line value used to report all ^{14}C ages ($b_{RL} = 2.00$). Note that many of the reactions reported here are enzymatically catalyzed and thus do not operate in equilibrium in nature; nonetheless, equilibrium isotope effects represent a useful limiting case when exploring the possible range of ^{14}C age offsets due to fractionation.

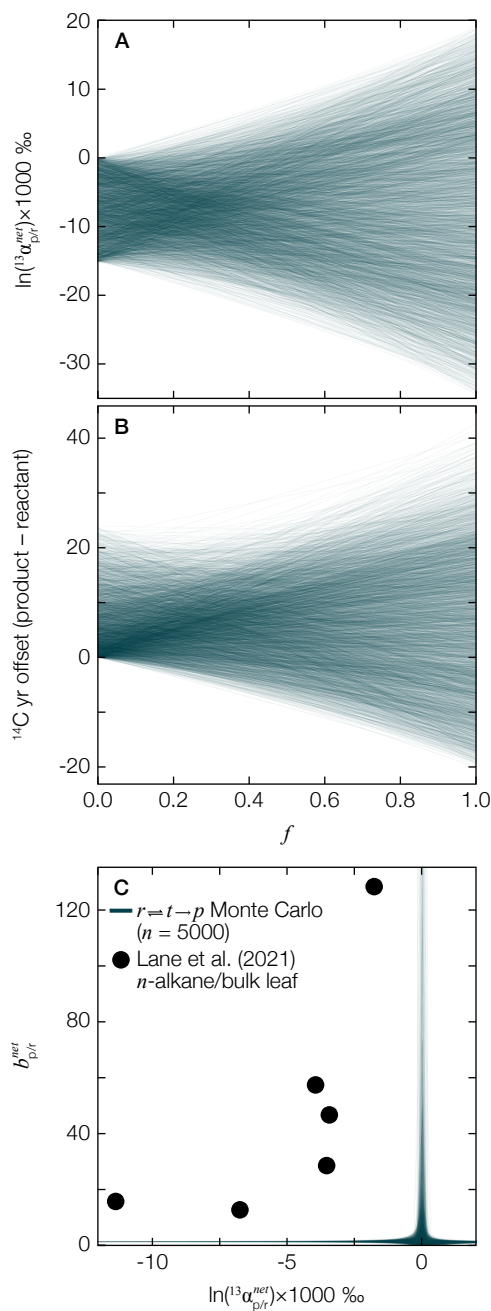


Figure 2: **Expressed isotope effects for a multi-step reaction network.** Monte Carlo results ($n = 5000$ iterations) for the reaction network $r \xrightleftharpoons[1]{} t \xrightarrow[2]{} p$ showing (A) $^{13}\alpha_{p/r}^{\text{net}}$ and (B) ^{14}C age offsets plotted as a function of f , the degree of reversibility for reaction step 1, and (C) $b_{p/r}^{\text{net}}$ plotted as a function of $^{13}\alpha_{p/r}^{\text{net}}$. Also shown in panel (C) are the calculated b values for n -alkane biosynthesis relative to bulk leaf tissue that would be required to explain the ^{14}C results of Lane et al. (2021) (Table 1). These values are clearly inconsistent with Monte Carlo predictions, even when considering that the model calculations performed here encompass all known values for all input parameters (Section 2.4) and are therefore expected to yield the broadest possible b range. In contrast to the interpretation of Lane et al. (2021), these results indicate that non-canonical b values are only possible at “crossover points” when $\ln(^{13}\alpha_{\text{net}}) \rightarrow 0$, as has been reported previously for other isotope systems (Bao et al., 2015).